Tunnelling and Underground Space Technology 95 (2020) 103141

Contents lists available at ScienceDirect

Tunnelling and Underground Space Technology

journal homepage: www.elsevier.com/locate/tust

A novel displacement back analysis method considering the displacement loss for underground rock mass engineering

Yan Zhang[a], Guoshao Su[b], Baochen Liu[a], Tianbin Li[c]

[a] Guangxi Key Laboratory of Geomechanics and Geotechnical Engineering, College of Civil Engineering and Architecture, Guilin University of Technology, Guilin 541004, China

[b] Key Laboratory of Disaster Prevention and Structural Safety of Ministry of Education, School of Civil and Architecture Engineering, Guangxi University, Nanning 530004, China

[c] State Key Laboratory of Geohazard Prevention and Geoenvironment Protection, Chengdu 610059, China

ARTICLE INFO

Keywords:
Underground engineering
Back analysis
Displacement loss

ABSTRACT

Most back analysis methods for geotechnical engineering are based on the measured displacement. However, before the monitoring sections are assembled, the displacement—termed the displacement loss—has already been induced; this displacement is difficult to determine, and thus, it is not considered in the back analysis. In the present study, a novel displacement back analysis method considering the displacement loss is developed, that can obtain not only the reasonable mechanical parameters of rock masses but also the displacement loss. To reduce the computational cost of back analysis, a new hybrid optimization algorithm based on the Gaussian process (GP) and particle swarm optimization (PSO) is presented. The GP is used as an inexpensive fitness evaluation surrogate to predict the global optimum solution and accelerate the local search of PSO, which is employed to determine the best mechanical parameters for the model. Combined with FLAC^{3D} numerical analysis, a novel back analysis method called GP-PSO-FLAC^{3D} is proposed. The results of a case study demonstrate that this method can effectively predict more reasonable mechanical parameters and displacement loss using the monitored displacement. An engineering application in the auxiliary tunnel of the Jinping II hydropower station indicates that the elastic deformation of the surrounding rock increases rapidly after excavation, especially for deep tunnels, thereby resulting in a large displacement loss. The back analysis results for the main powerhouse of the Taian pumped storage power station indicate that the displacement loss also exists in engineering processes involving ordinary geostress conditions. Therefore, the displacement loss of a surrounding rock mass cannot be ignored in the stability evaluation or back analysis of underground engineering, especially for deep underground rock engineering.

1. Introduction

It is well known that design input parameters such as the rock mass strength and in situ stress are critical for underground excavation engineering design. The rationality of rock mass parameter selection can directly affect the rationality of the evaluation results of the rock mass stability. If unsuitable parameters are used for engineering design, critical losses of human lives and property may occur (Hoek and Diederichs, 2006; Bieniawski, 1984; Cai, 2011; Barton et al., 1974).

Conventionally, the design input parameters are obtained by conducting several in situ tests (i.e., block shear tests and plate-loading tests) for different points under the conditions of complex topography and geology, which is not only a time-consuming and expensive process but also an unrepresentative method for the overall rock mass (Cai et al., 2007; Gioda and Sakurai, 1987). Compared with traditional in situ tests, back analysis methods have numerous advantages, which include an easier implementation, a considerably lower cost, and a higher efficiency, and thus, these methods have been widely used to solve the problem of obtaining the design input parameters. Back analysis methods can make full use of the in situ monitoring displacement to deduce the mechanical parameters of rock masses (Feng et al., 2000), in situ stress field (Sakurai and Takeuchi, 1983; Kaiser et al., 1990), excavation parameters (Rechea et al., 2008) and numerous other input parameters (Pirulli and Mangeney, 2008; Berti et al., 2017). Back analysis methods can be classified into two major types based upon different calculation methods: analytical and numerical methods (Feng et al., 1999). Since the analytical method is applicable only to back analysis problems involving simple geometric shapes and boundary conditions, it is difficult to adopt for complex geotechnical engineering; thus, numerical methods, which have more adaptability, have been widely used. Generally, to obtain more suitable input parameters, the numerical back analysis problem is transformed into an optimization problem, in which the error between the computed displacement and actual measured displacement is regarded as the optimization objective

https://doi.org/10.1016/j.tust.2019.103141
Received 22 February 2019; Received in revised form 29 June 2019; Accepted 6 October 2019
Available online 21 October 2019
0886-7798/

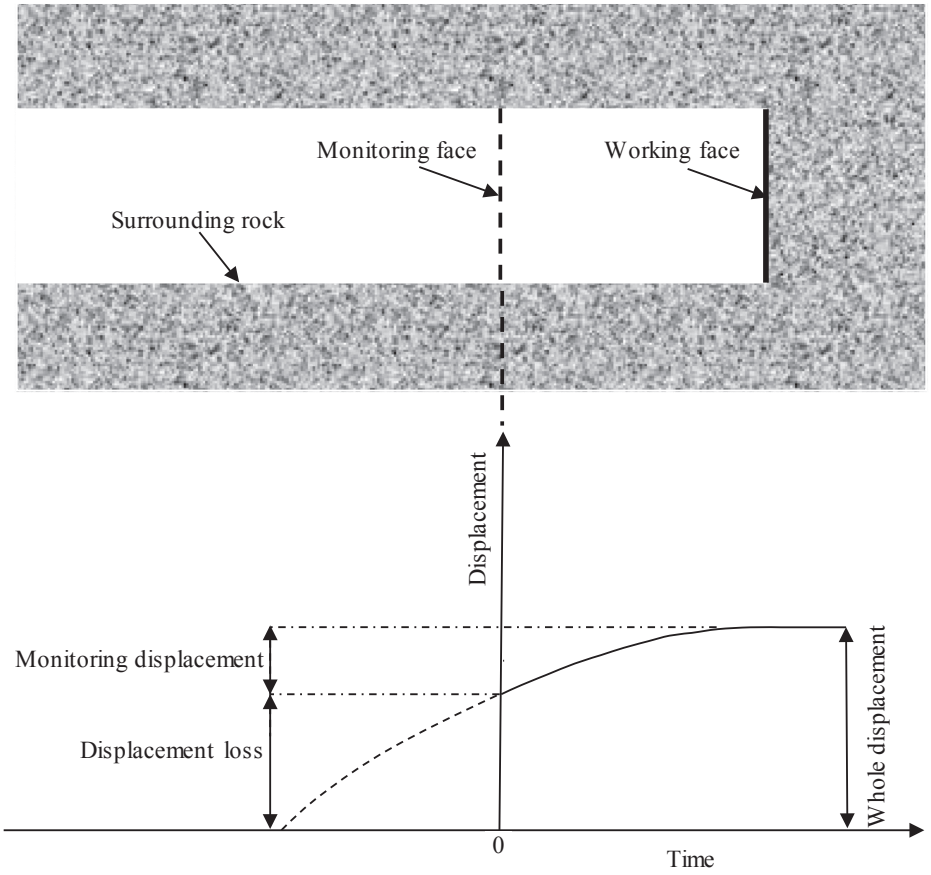

Fig. 1. Profile of radial displacement in the vicinity of the working face.

function and the different input parameters are regarded as the optimization variables. Then, various optimization methods can be employed to solve the problem (Yang et al., 2010; Tang and Kung, 2009; Hao et al., 2016).

The displacement of the surrounding rock often occurs before monitoring instruments have been assembled; hence, it is termed the displacement loss (Fig. 1). Currently, the computed displacement is obtained by a numerical simulation, which represents the displacement for the entire process. However, the actual measured displacement that is compared with the computed displacement is only a part of the actual overall displacement. Because the monitoring sections are always assembled after the working face excavation, considerable displacement loss is involved in the displacement monitoring of underground rock mass engineering. In particular, for deep tunnels under high in situ stresses, the rock stress is suddenly released at the moment of excavation, and the displacement loss is induced subsequently. The value of the displacement loss may not be extremely large; however, it may represent a large proportion of the overall displacement. If the measured displacement, which is a lower value than the actual one, is regarded as the actual whole displacement and compared with the computed displacement, it will inevitably lead to a significant deviation in the back analysis results. In addition, since the emergence of the New Australian Tunneling Method (NATM) construction concept, the use of surrounding rock displacement measurement information for information-based construction has become popular in modern tunnel construction (Farias et al., 2004; Mohammadi et al., 2014; Yu et al., 2016). During information-based construction, if the displacement loss information is ignored, the construction safety may be adversely impacted. Therefore, methods to obtain the displacement loss and incorporate it into the back analysis represent a key problem in evaluating the surrounding rock stability and ensuring the safety of construction especially for deep tunnels.

For several years, the consideration of the displacement loss has relied on the displacement (or load) release coefficient. When the coefficient is determined by experience, the corresponding equivalent release displacement can be obtained (Cai et al., 2002; Lu et al., 2014). However, this method involves some uncertainties due to the experientially determined coefficient. Recent literature reports only one method of directly obtaining the displacement loss, in which the Hoek experiential formula is applied and the monitoring displacement is used to calculate the displacement loss (Zhang et al., 2009). Because this method is based on an experiential formula and involves many assumptions, such as those for the continuity and homogeneity of the rock mass, it can obtain the displacement loss only for the two-dimensional planar problem. Thus, the existing theories and methods cannot fully satisfy the requirements of engineering practice. It is therefore necessary to determine a more reasonable and effective method for obtaining the displacement loss of the surrounding rock.

The actual monitored displacement is the most direct and effective information obtained during tunnel excavation. Determining the displacement loss using the monitored displacement is an effective method. Accordingly, this paper proposes a novel displacement back analysis method considering the displacement loss based on the monitored displacement.

As mentioned earlier, many optimization methods can solve the back analysis problem for the displacement loss. However, a rock mass under complex conditions may be cut into both a continuous and a discontinuous body by all types of geologic structures. Thus, the optimization objective function of optimization back analysis is usually a complex nonlinear multimodal function. The traditional gradient optimization method can obtain only a local optimal solution (Zhao and Yin, 2009; Khamesi, 2015). In recent years, a number of stochastic

search optimization methods have been proposed to solve this problem. These include the evolution strategy (ES) (Moreira et al., 2013), genetic algorithm (GA) (Levasseur et al., 2010; Beiki et al., 2013; Hashash et al., 2010), particle swarm optimization (PSO) (Gao, 2006; Knabe et al., 2012; Hajihassani et al., 2018) and ant colony optimization (ACO) (Lin et al., 2014; Gao and Feng, 2005). These methods evaluate the objective function in a random sample of points from the search space and subsequently manipulate the sample. To determine the best sample, thousands of fitness evaluations must be performed. However, in practical engineering, a single exact fitness evaluation involving the numerical analysis of a complex engineering system often consumes many minutes or hours of CPU time, which makes application of the stochastic search optimization method to practical engineering infeasible.

One promising way to significantly reduce the computational cost of stochastic search optimization methods is to employ a computationally inexpensive surrogate model in place of computationally expensive exact fitness evaluations. Research on surrogate-assisted evolutionary computation began over a decade ago and has received increasing interest in recent years (Ninić et al., 2017; Li et al., 2014; Miro et al., 2015). In the surrogate approach, a surrogate model is trained on the existing evaluated individuals (fitness cases) in order to guide the search for promising solutions. By leveraging the surrogate models, the number of expensive fitness evaluations decreases, which results in a significant decrease in the computational cost (Brigham and Aquino, 2007; Ninić and Meschke, 2015).

In this paper, to effectively reduce the number of fitness evaluation and improve the efficiency of the displacement loss back analysis, a Gaussian process (GP) surrogate-assisted PSO algorithm is proposed. Through a combination with FLAC^{3D} (Itasca Consulting Group, Inc., 2005), which is a famous geotechnical numerical simulation software (Zhang et al., 2008; Wang et al., 2018), a new back analysis optimization method called GP-PSO-FLAC^{3D} is developed. The remainder of this paper is structured as follows. Section 2 provides a brief introduction of the displacement back analysis method considering the displacement loss. Section 3 presents the GP-PSO-FLAC^{3D} method. Section 4 demonstrates the validity and efficiency of the proposed method by using numerical experiments. Section 5 describes the engineering application, and the conclusions of this study are stated in Section 6.

2. Displacement back analysis method considering the displacement loss

2.1. General concept

For a given tunnel, with the help of a numerical computation model, we can easily obtain the curve for the whole displacement with time at a certain measurement point of the surrounding rock after excavation; this curve is the total computation convergence displacement curve. If the mechanical parameters for the numerical computation model are different, a different total computation convergence displacement curve will be obtained. The computation convergence displacement curve is then depicted in the same coordinate system as the measured displacement according to the corresponding monitoring time. For example, two different total computation convergent displacement curves are shown in Fig. 2. These curves are divided into two parts based on the actual displacement monitoring time: one part is the displacement loss (dashed line) and the other part is the monitoring displacement (solid line). As seen from Fig. 2, compared with computation curve 1, the monitoring part of computation curve 2 is more similar to the actual monitoring displacement curve. Therefore, it can be considered that computation curve 2 has a higher reliability, and the corresponding displacement loss for this curve is regarded as the possible displacement loss. Because the displacement loss is considered in this case, the mechanical parameters of curve 2 are regarded as more reasonable input parameters, which can more accurately simulate an actual engineering project. Next, the key problem is how to obtain the mechanical parameters of curve 2. We can use the optimization back analysis method to determine the mechanical parameters of curve 2, and the problem of obtaining the displacement loss is then transformed into an optimization back analysis problem.

2.2. Mathematical model of optimization back analysis

The minimization of error between the computation displacement curve and monitoring displacement curve is regarded as the optimization objective. The mechanical parameters of the surrounding rock are regarded as the decision variables. By optimizing the parameters, the total computation displacement curve, which is the most similar to the actual monitoring displacement curve, is determined. The displacement loss of this curve is regarded as being relatively credible.

To evaluate the similarity between the two curves, the monitoring points and monitoring time are determined for comparison. Consequently, the optimization objective function, which is also called the fitness function, can be set as in Eq. (1):

$$\min f(\boldsymbol{x}) = \sum_{i=1}^{n}\sum_{t=1}^{m}[d_{it}(\boldsymbol{x}) - \bar{d}_{it}]^2 \tag{1}$$

where $f(\boldsymbol{x})$ is the objective function, $\boldsymbol{x}$ represents the decision variables, m is the total monitoring time, n denotes the total monitoring points, d_{it} is the computational displacement for monitoring point i at moment t, and $\bar{d}_{it}$ is the actual monitoring displacement for monitoring point i at moment t.

The constraint is presented by Eq. (2):

$$a \leqslant x \leqslant b \tag{2}$$

where the constants a and b respectively indicate the lower and upper limits for the decision variables, constituting the reasonable range of the mechanical parameters in practical engineering. The reasonable range of the parameters can not only reduce the computational cost, but also increase the accuracy of the back analysis results. Generally, it is determined on the basis of laboratory measurements.

After establishing the optimization objective function and constraint condition, any optimization method can be used to solve this optimization problem. In this study, we use the GP-PSO-FLAC^{3D} optimization method to address this issue. The details of the proposed method are presented in the next section.

3. A displacement loss back analysis method using GP-PSO-FLAC^{3D}

3.1. GP

In this work, the GP model is selected as the surrogate model, which is a newly developed machine learning technology based on strict theoretical fundamentals and Bayesian theory (Seeger, 2004). In recent years, the GP has attracted much attention in the machine learning community and has been widely applied (Hensman et al., 2010; Su et al., 2007; Pal and Deswal, 2010; Jadaliha et al., 2013).

Compared to an artificial neural network (ANN), which is the most prominent surrogate model, the main advantage of the GP is its simplicity: neither a network size nor a topology must be selected. In addition, the GP can automatically choose the optimum hyperparameters. More details concerning the GP can be found in the work by Rasmussen (Rasmussen, 2006).

The GP is a collection of random variables, any finite set of which has a joint Gaussian distribution. The GP is completely specified by its mean function $m(\boldsymbol{x})$ and the covariance function $k(\boldsymbol{x}, \boldsymbol{x}')$ as follows:

$$f(\boldsymbol{x}) \sim GP(m(\boldsymbol{x}), k(\boldsymbol{x}, \boldsymbol{x}')) \tag{3}$$

A training set $\boldsymbol{D}$ of s observations exists as $\boldsymbol{D} = \{(\boldsymbol{x}_i, y_i) | i = 1, \ldots s\}$,

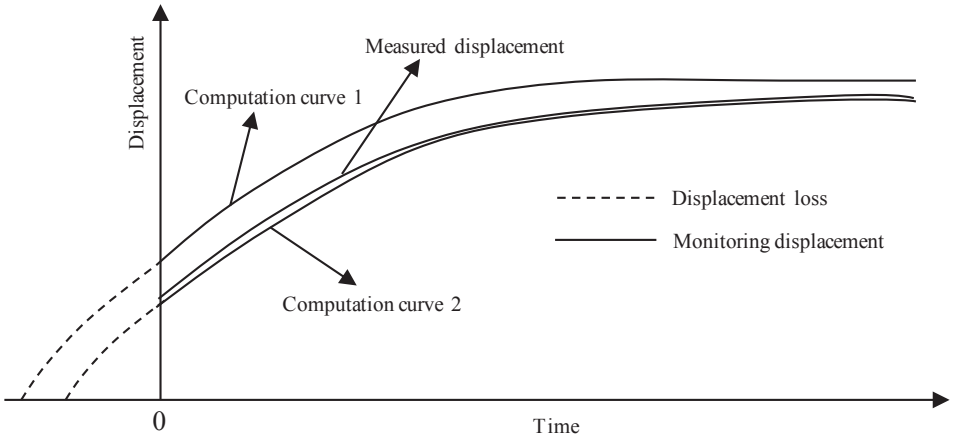

Fig. 2. Computation convergence displacement and measured displacement curves of the surrounding rock.

Begin
Randomly generate the N particles of 1st generation
Evaluate the fitness of particles using objective function
Find the optimum particle p_{id} and global optimum particle p_{gd}
$p = 0$
While termination criteria is not met
Generate N particles of (2+p)th generation using Eq. 10
Evaluate the fitness of these particles using the objective function

The (2+p)×N particles are sorted according to an increasing order of fitness
The upper 2×N particles and their fitness are selected to establish the training datasets

Train the GP by the training datasets
Update the optimum particle p_{id} and global optimum particle p_{gd} at the current iteration

For i=1, k
Generate N particles using Eq. 10
Evaluate the fitness of N particles using the trained GP
End For

Find the best particle with the minimum fitness in k generations
Evaluate its fitness using the objective function and replace its fitness evaluated using the trained GP
Compare this fitness to $gbest$, select the smaller one as the global optimum particle p_{gd} and update $gbest$
Replace the worst particle with the maximum fitness in training datasets by this particle and its fitness

$p = p$+1
End While
End

Fig. 3. Pseudocode of GP-PSO.

Table 1
Parameter settings of the benchmark functions.

Function	Formulation	Trait	Minimal function value	Search space
Sphere	$f(x) = \sum_{i=1}^{n} x_i^2$	Unimodal	0	$[-2,2]^{30}$
Rastrigin	$f(x) = \sum_{i=1}^{n} (x_i^2 - 10\cos(2\pi x_i)+10)$	Multimodal	0	$[-2,2]^{30}$

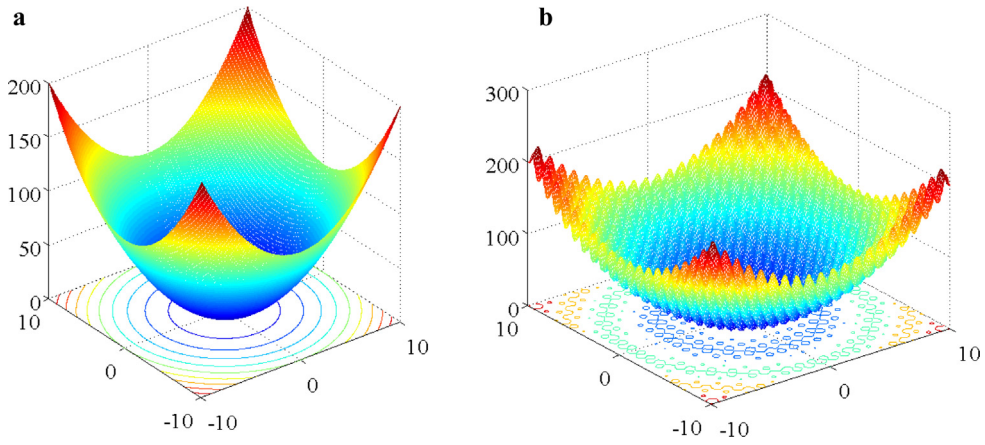

Fig. 4. 3D graphs for benchmark functions (**a:** Sphere function; **b:** Rastrigin function).

Table 2
Parameter settings of GP-PSO and PSO.

Function	D	N	lb	ub	t_{max}	$\boldsymbol{v}_{max}$	c_1	c_2	k	Accuracy
Sphere	30	50	−2	2	20,000	1	2	2	10	1.00E−03
Rastrigin	30	50	−2	2	50,000	1	2	2	10	3.00E+01

Table 3
Comparison between the number of function evaluations for GP-PSO and PSO.

Function	PSO	GP-PSO
Sphere	427,400	32,129
Rastrigin	802,050	10,862

where $\boldsymbol{x}$ denotes an input vector and y denotes the scalar output or target. The goal of Bayesian forecasting is to compute the distribution $p(y_* | \boldsymbol{x}_*, \boldsymbol{D})$ of output y_* given a test input $\boldsymbol{x}_*$ and a set of training points $\boldsymbol{D}$. Using the Bayesian rule, the posterior distribution for the GP outputs y_* can be obtained. By conditioning the observed targets in the training set, the predictive distribution is Gaussian:

$$y_* | \boldsymbol{x}_*, \boldsymbol{X}, \boldsymbol{y} \sim N(\bar{y}(\boldsymbol{x}_*), \bar{\sigma}(\boldsymbol{x}_*)) \tag{4}$$

where the mean and variance are given by

$$\bar{y}(\boldsymbol{x}_*) = \boldsymbol{k}_*^T (\boldsymbol{K} + \sigma_n^2 \boldsymbol{I})^{-1} \boldsymbol{y} \tag{5}$$

$$\bar{\sigma}^2(\boldsymbol{x}_*) = k(\boldsymbol{x}_*, \boldsymbol{x}_*) - \boldsymbol{k}_*^T (\boldsymbol{K} + \sigma_n^2 \boldsymbol{I})^{-1} \boldsymbol{k}_* \tag{6}$$

where a compact form of the notation for the matrix of the covariance functions is $\boldsymbol{k}_* = \boldsymbol{K}(\boldsymbol{X}, \boldsymbol{x}_*)$, $\boldsymbol{K} = \boldsymbol{K}(\boldsymbol{X}, \boldsymbol{X})$, and σ_n^2 is the unknown variance of the Gaussian noise.

The GP procedure can handle complex models by simply using a covariance function with an exponential term:

$$\boldsymbol{k}(\boldsymbol{x}_p, \boldsymbol{x}_q) = \sigma_f^2 \exp\left(-\frac{\|\boldsymbol{x}_p - \boldsymbol{x}_q\|^2}{2\boldsymbol{l}^2}\right) + \sigma_n^2 \delta_{pq} \tag{7}$$

where $\boldsymbol{l}$ is the length-scale vector, σ_f^2 is the signal variance, and δ_{pq} is a Kronecker delta function. This function expresses the concept that nearby inputs have highly correlated outputs. The GP employs a set of hyperparameters $\boldsymbol{\theta}$, including the length-scale $\boldsymbol{l}$, the signal variance σ_f^2, and the noise variance σ_n^2. The hyperparameters $\boldsymbol{\theta}$ can be optimized based on a log-likelihood framework:

$$L = \log p(\boldsymbol{y}|\boldsymbol{X}, \theta) = -\frac{1}{2}\boldsymbol{y}^T \boldsymbol{C}^{-1} \boldsymbol{y} - \frac{1}{2}\log\det \boldsymbol{C} - \frac{n}{2}\log 2\pi \tag{8}$$

The log-likelihood and its derivative with respect to $\boldsymbol{\theta}$ can be expressed as

$$\frac{\partial L}{\partial \theta} = -\frac{1}{2} tr\left(\boldsymbol{C}^{-1}\frac{\partial \boldsymbol{C}}{\partial \theta}\right) + \frac{1}{2}\boldsymbol{y}^T \boldsymbol{C}^{-1}\frac{\partial \boldsymbol{C}}{\partial \theta}\boldsymbol{C}^{-1}\boldsymbol{y} \tag{9}$$

where $\boldsymbol{C} = \boldsymbol{K} + \sigma_n^2 \boldsymbol{I}$.

The hyperparameters $\boldsymbol{\theta}$ are initialized to random values in a reasonable range, and subsequently, the algorithm searches for the optimal values by using an iterative method such as the conjugate gradient.

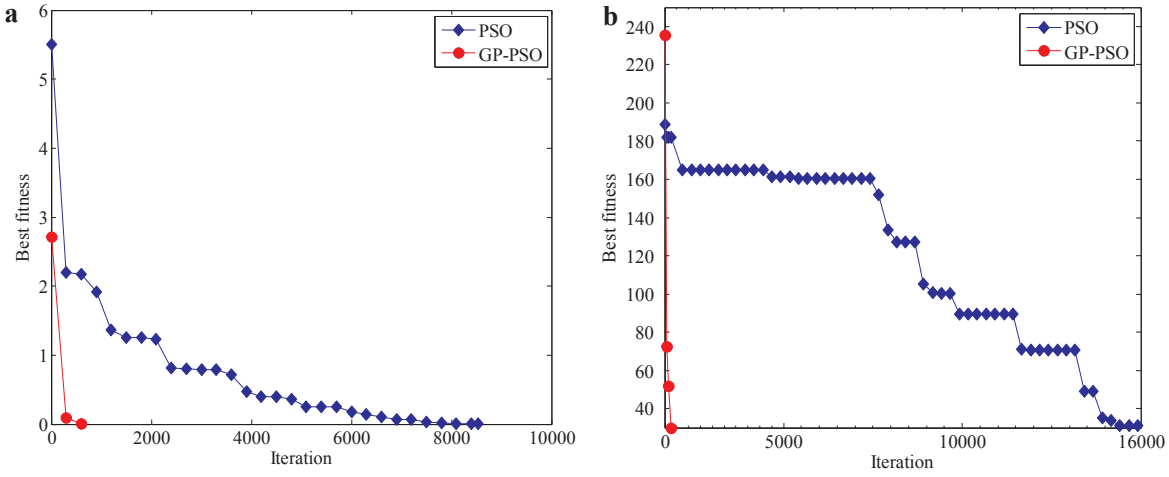

Fig. 5. Comparison of the convergence between GP-PSO and PSO (**a:** Sphere function; **b:** Rastrigin function).

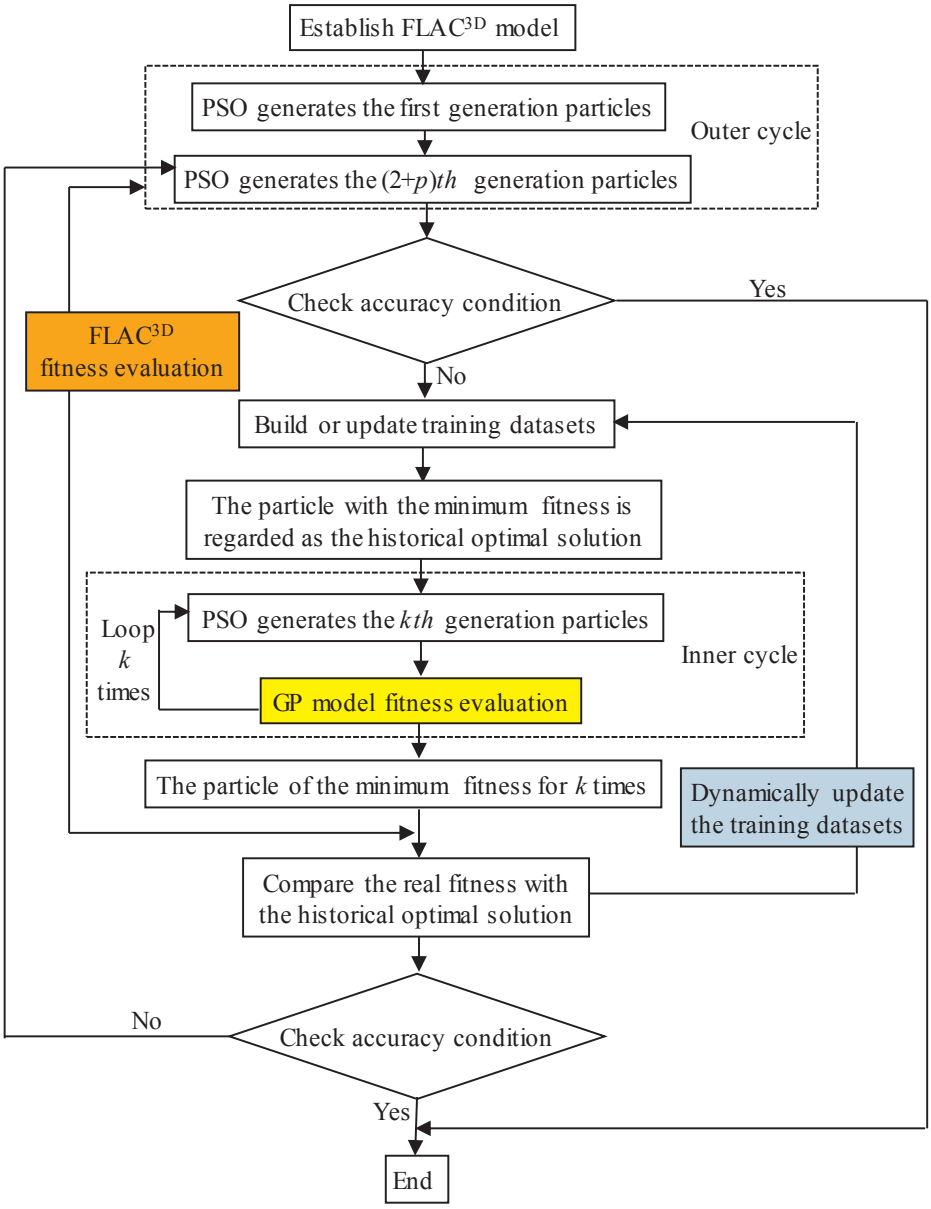

Fig. 6. Schematic of the process flow of the GP-PSO-FLAC^{3D} method.

3.2. PSO

The PSO model is initialized with a population of random solutions, and it searches for the optima by updating generations (Eberhart and Kennedy, 1995). In PSO, the potential solutions, called particles, fly through the problem space by following the current "optimum" particles. There are two optimum particles. One keeps track of the coordinates associated with the best solution in the current stage, and the best solution is defined as *pbest*. The other optimal solution tracked by the particle swarm optimizer is obtained at an instant by considering any particle in the neighboring region of the particle; when a particle takes the entire population as its topological neighbors, this global best is denoted as *gbest*. With the help of the two optimal values, the particle updates its velocity and positions as per the following equations:

$$\left.\begin{aligned} v_{i\,d} &= w v_{i\,d} + c_1 r_1 (p_{i\ \ d} - x_{id}) + c_2 r_2 (p_{g\,d} - x_{id}) \\ x_{id} &= x_{id} + v_{id} \end{aligned}\right\} \tag{10}$$

where $\boldsymbol{v}_{id}$ is a velocity vector and $\boldsymbol{x}_{id}$ is a position vector. p_{id} represents the best position of particle i, and its fitness is *pbest*. p_{gd} corresponds to the global best position in the process of particle iteration on the *d-th* dimension and its fitness is *gbest*. The parameters r_1 and r_2 are two random values uniformly distributed in [0, 1] (Feng et al., 2006). c_1 and c_2 are acceleration constants usually defined as $c_1 = c_2 = [1.8, 2.0]$ (Wang and Ma, 2017). The parameter w is the inertial weight, which controls the influence of the previous velocity on the new velocity. The inertial weight w can be determined as in Eq. (11):

$$w = w_{\max} - \frac{w_{\max} - w_{\min}}{t_{\max}} t \tag{11}$$

where t is the current iteration step, $t_{\max}$ is the maximum iteration step, $w_{\max}$ is the maximum inertial weight, and $w_{\min}$ is the minimum inertial weight. Usually, $w_{\max} = 0.9$ and $w_{\min} = 0.4$ (Li et al., 2014; Ojha and Das, 2012).

3.3. GP surrogate-assisted PSO

During the optimization back analysis of parameters, a single exact fitness function evaluation often requires several minutes to hours, particularly for the analysis of a complex engineering system based on a

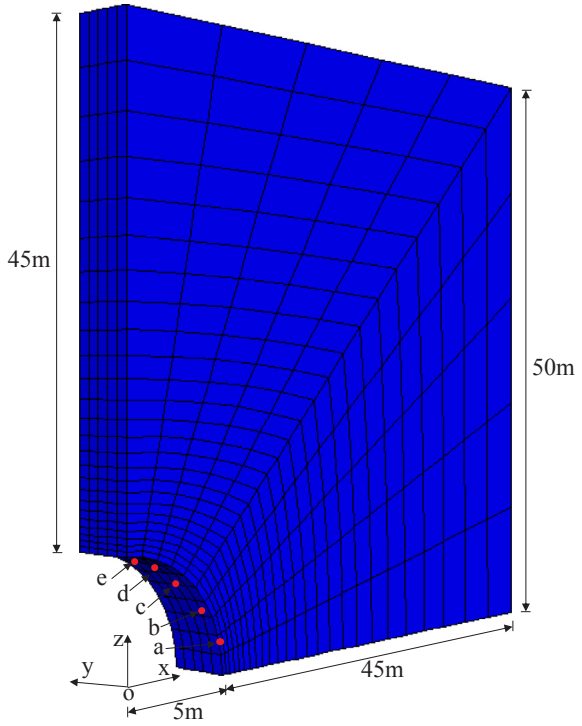

Fig. 7. 3D finite difference mesh and 5 monitoring points of one-fourth of the tunnel.

Table 4
Locations of monitoring points for the case.

Monitoring point number	*y* direction (m)	Toroidal angle (°)
a	0	15
b	1	30
c	2	45
d	3	60
e	4	75

numerical simulation. This high computational cost poses a serious impediment to the successful application of PSO. To improve the efficiency of PSO for computationally expensive optimization problems, a GP-based PSO algorithm is developed. In the GP-PSO algorithm, the GP model is used as the surrogate model to approximate the real fitness function. Once the approximation fitness function is established, we can directly use the approximation function instead of the real function to evaluate the fitness of the particles. Hence, the number of real function evaluations can be reduced considerably by using PSO to solve the optimization problem. The key points of the GP-PSO algorithm are as follows:

- Accelerated searching based on an approximation of the fitness function by GP

To accelerate the local search of PSO, once the *pbest* and *gbest* particles in each iterative step are found, some new particles are generated using Eq. (10), and their fitness is estimated by the trained GP. Subsequently, the best value with the minimum fitness is selected. To eliminate the predictive error of the fitness evaluated by GP approximation, the fitness of the best particle is evaluated again using the real function. If the real fitness of the best particle is less than *gbest*, it becomes the global best in the current iterative step, and *gbest* is replaced by its fitness. Thus, the number of real function evaluations in the exploration process is only one because the fitness of the new particles, with the exception of the best one, is evaluated by the trained GP rather than a real function. Consequently, the computational cost of the accelerated search process is low.

- Dynamically updating the training datasets to improve the approximation quality of the GP model

The accuracy of the GP-PSO algorithm depends on the appropriateness of the generated GP model; however, in terms of the prediction, the accuracy of the GP model in interpolation and validation depends highly on the quality of the training datasets. To avoid excessively relying on the initial training datasets and to improve the quality of training datasets gradually in the exploration process, the datasets for training GP are updated dynamically in the GP-PSO algorithm. Thus, the training datasets are always consistent with the elite group of particles, and the quality of the general approximation of the GP model can be enhanced in the optimization process.

The specific implementation steps of the GP-PSO are shown as follows:

Step 1: Generate N particles in the 1*st* generation, in which the particles are randomly distributed throughout the design space and are bounded by specified limits. N is the population size of PSO, and it is usually determined by the dimension of the optimization problem.
Step 2: Evaluate the fitness of particles of the 1*st* generation by the objective function (i.e., real function or numerical computation). Find the optimum particle p_{id} and global optimum particle p_{gd}.
Step 3: Generate N particles of the $(2 + p)th$ generation using Eq. (10). Evaluate the fitness of these particles using the objective function.
Step 4: Sort the $(2 + p) \times N$ particles according to an increasing order of fitness, and select the upper limit $2 \times N$ particles and their fitness to establish the training datasets.
Step 5: Train the GP by the training datasets. Use the GP to approximate the objective function according to Eq. (5).
Step 6: Update the optimum particle p_{id} and global optimum particle p_{gd} at the current iteration.
Step 7: Generate N particles using Eq. (10) and evaluate the fitness of N particles using the trained GP. Find the best particle with the minimum fitness in k generations, where k can further optimize the best particle. k is determined by the complexity of the objective function; a more complex objective function corresponds to a larger value of k. Evaluate the fitness of this particle using the objective function and replace the fitness evaluated using the trained GP. Compare this fitness to *gbest*; then, select the smaller value as the global optimum particle p_{gd} and update *gbest*.
Step 8: Replace the worst particle with the maximum fitness in the

Table 5
Comparison of the results obtained with GP-PSO-FLAC^{3D} and PSO-FLAC^{3D}.

Method	The results of back analysis			The assumed real parameters			The relative errors (%)			The times of fitness evaluation	Computing time (s)
	μ	E (GPa)	η (GPa·d)	μ	E (GPa)	η (GPa·d)	μ	E (GPa)	η (GPa·d)		
PSO-FLAC^{3D}	0.260	4.866	9.915	0.250	5.000	10.000	4.160	2.680	0.850	600	1480
GP-PSO-FLAC^{3D}	0.239	5.038	10.298	0.250	5.000	10.000	4.440	0.760	2.980	185	448

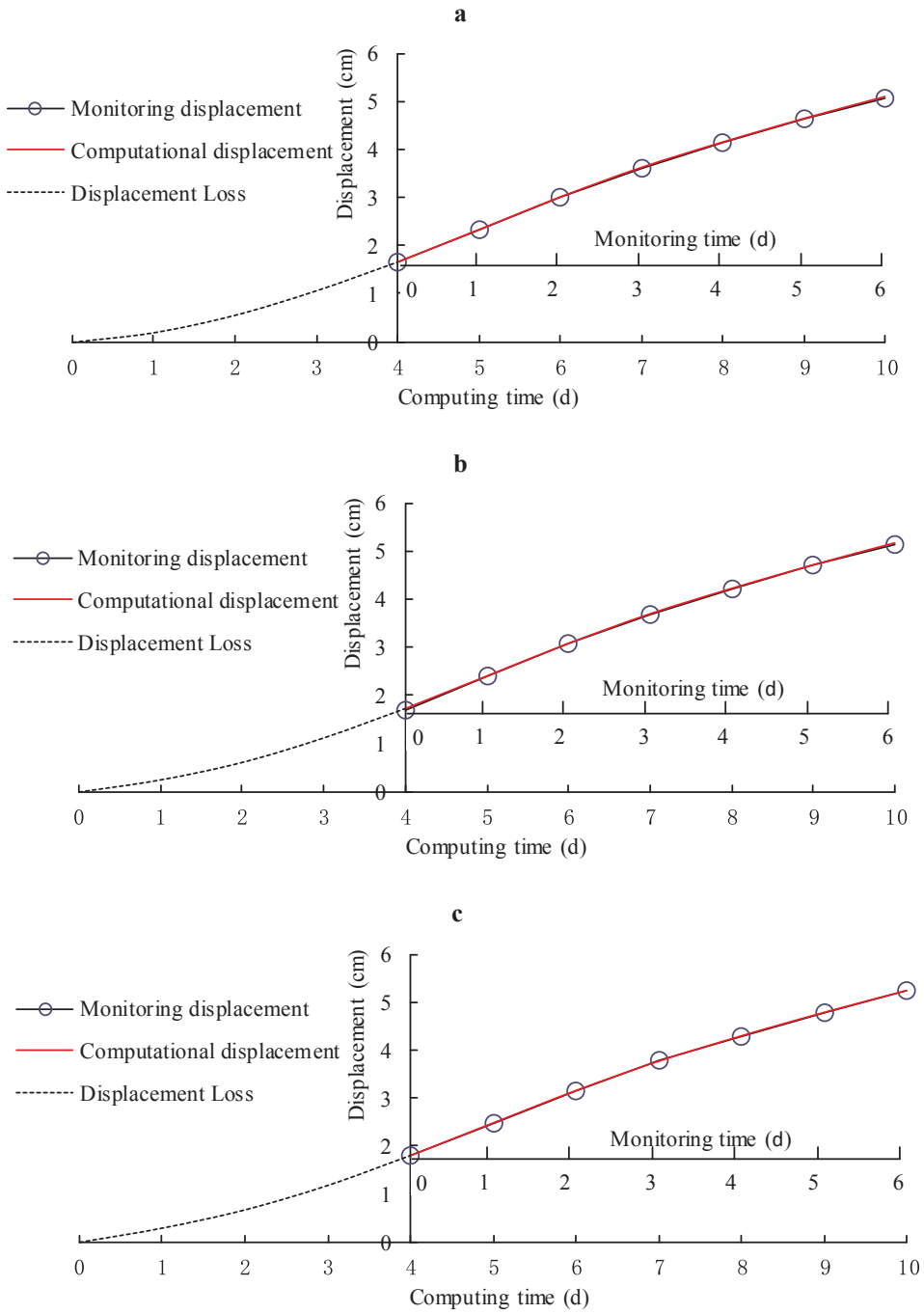

Fig. 8. Comparison between the computational displacement and monitoring displacement of the 5 monitoring points for the case.

training datasets by this particle and its fitness.

Step 9: Repeat **Steps 3–8** until the termination criterion is met. For the current implementation, the termination criterion is defined based on the maximum number of iterations reached or the accuracy satisfied.

The pseudocode of the GP-PSO algorithm is given in Fig. 3. A MATLAB-based program was developed accordingly.

The performance of the GP-PSO algorithm was compared to that of the conventional PSO algorithm by evaluating the convergence velocity and efficiency for the benchmark optimization problem. One unimodal function and another multimodal benchmark function are selected, as given in Table 1. The minimal function value is $f = 0$, and the search space is confined to $[-2, 2]^{30}$; here, 30 denotes the dimension of the functions. The graphs for the two functions in the 3-dimensional cases are shown in Fig. 4. The Sphere function is unimodal, convex and differentiable without flat regions. The Rastrigin function is a famous highly multimodal test function that is usually used to evaluate the efficiency of an optimization algorithm (Digalakis and Margaritis, 2004; Evers and Ghalia, 2009; Karaboga and Basturk, 2008).

The PSO parameters include the dimension (D), population size (N), lower (lb) and upper (ub) bounds of the search space, maximum number of iterations (t_{max}), maximum velocity of the particle ($\boldsymbol{v}_{max}$), and acceleration constants (c_1 and c_2). In addition to these, another parameter is critical for the GP-PSO algorithm, namely, the maximum number of GP circular k. All the parameter settings are listed in Table 2.

For the benchmark functions, we measure the number of real function evaluations required to achieve the expected accuracy. To be

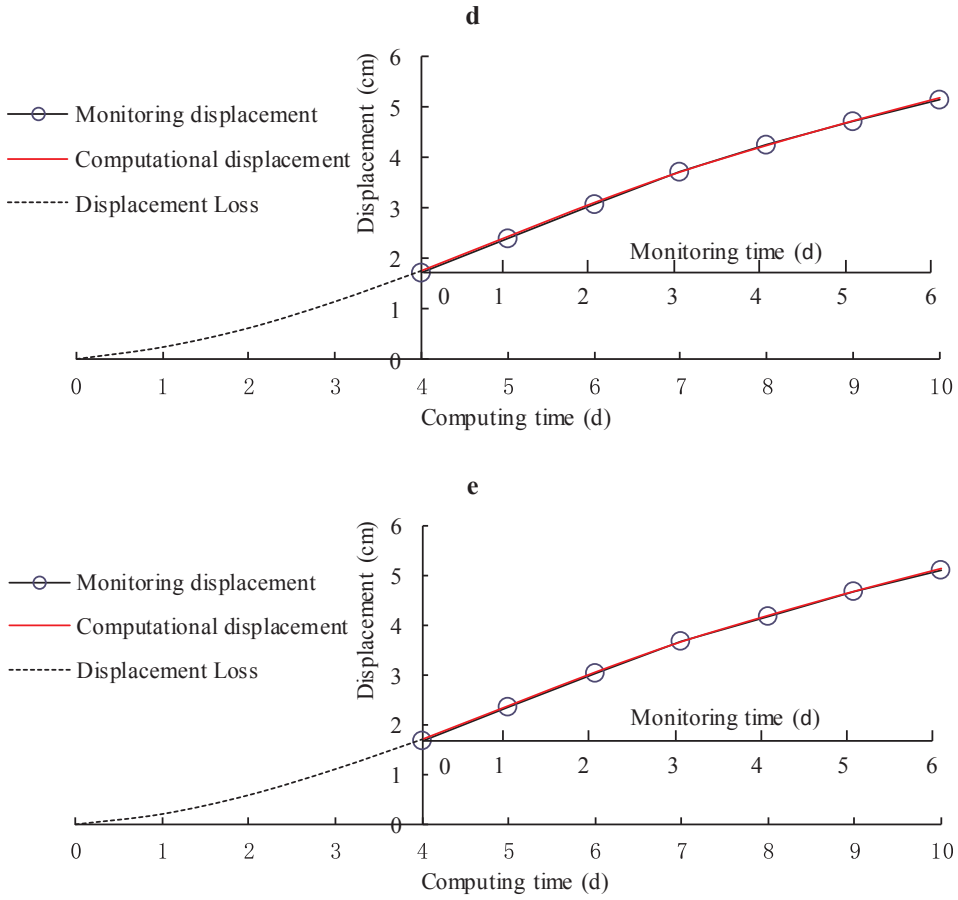

Fig. 8. (*continued*)

Table 6
Comparison between the computational displacement loss and assumed displacement loss.

Monitoring point number	Computational displacement loss (cm)	Assumed displacement loss (cm)	The relative errors (%)
a	1.652	1.642	0.609
b	1.709	1.708	0.059
c	1.777	1.787	0.560
d	1.729	1.733	0.231
e	1.695	1.689	0.355

fair, all the different algorithms are forced to use the same accuracy as the termination criterion; for different functions, a different accuracy for the termination criterion is assumed, as shown in Table 2.

The program for all experiments is run 30 times independently; next, the number of function evaluations is averaged. The total numbers of real function evaluations using GP-PSO and PSO are listed in Table 3. It can be seen that the total number of real function evaluations for GP-PSO is much less than that for PSO. For the Sphere function, the average multiple of the real function evaluation is more than 13 times. For the more complex Rastrigin function, the average multiple is close to 74 times. The efficiency of GP-PSO is much higher than that of PSO, especially for the complex problem.

To provide a visual and straightforward comparison between the proposed GP-PSO algorithm and PSO, a comparison of the performances of GP-PSO and PSO for the two functions is shown in Fig. 5, from which the convergence trends of the variants of PSO and GP-PSO in a random run can beidentified. Fig. 5 also shows that the GP-PSO algorithm converged more rapidly towards the optimal solution than did the PSO algorithm.

The above discussion indicates that the proposed GP-PSO algorithm is much more efficient than PSO in terms of achieving an identical

Table 7
Comparison of the results obtained with different monitoring time.

Monitoring point	Monitoring from the last 6 days			Monitoring from the last 4 days			Monitoring from the last 2 days		
	Computational displacement loss (cm)	Assumed displacement loss (cm)	The relative errors (%)	Computational displacement loss (cm)	Assumed displacement loss (cm)	The relative errors (%)	Computational displacement loss (cm)	Assumed displacement loss (cm)	The relative errors (%)
a	1.654	1.642	0.731	2.972	3.001	0.966	4.042	4.147	2.532
b	1.693	1.708	0.878	3.035	3.071	1.172	4.131	4.217	2.039
c	1.797	1.787	0.560	3.135	3.155	0.634	4.223	4.301	1.814
d	1.737	1.733	0.231	3.122	3.098	0.775	4.190	4.244	1.272
e	1.699	1.689	0.592	3.074	3.049	0.820	4.155	4.196	0.977

Note that the total computing time is 10 days.

Table 8
Comparison of the results obtained with different monitoring points for the monitoring time of 6 days.

Monitoring point	Assumed displacement loss (cm)	Computational displacement loss (cm)					
		1 point	The relative errors (%)	3 points	The relative errors (%)	5 points	The relative errors (%)
a	1.642	1.602	2.436	1.676	2.071	1.654	0.731
b	1.708	1.675	1.932	1.733	1.464	1.693	0.878
c	1.787	1.773	0.783	1.799	0.672	1.797	0.560
d	1.733	1.753	1.154	1.742	0.519	1.737	0.231
e	1.689	1.725	2.131	1.702	0.770	1.699	0.592

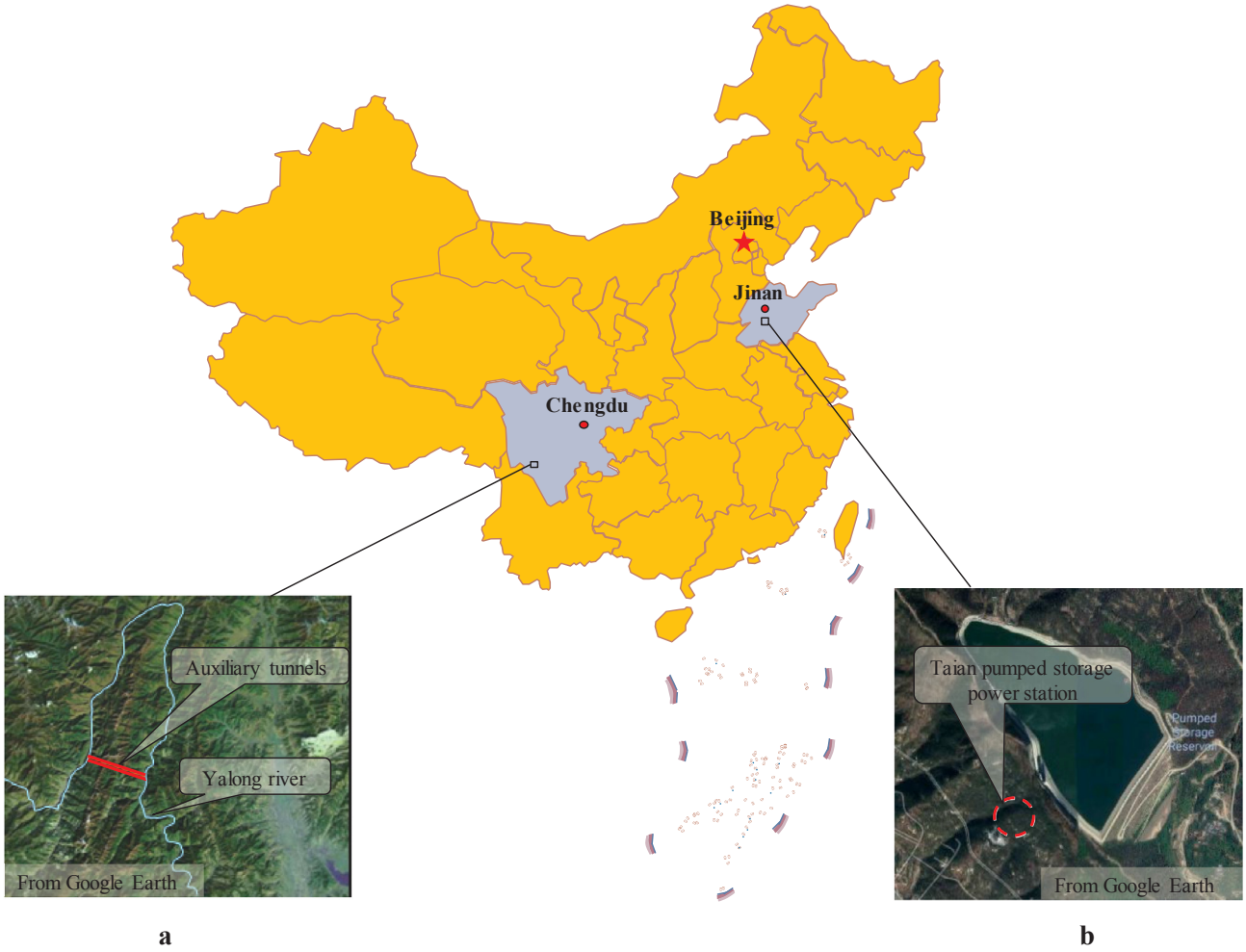

Fig. 9. Locations of the auxiliary tunnels for the Jinping II hydropower station and the Taian pumped storage power station in China (**a:** the auxiliary tunnels for the Jinping II hydropower station; **b:** the Taian pumped storage power station).

accuracy.

3.4. GP-PSO-FLAC^{3D}

In an actual project, based on the GP-PSO algorithm, PSO is used to randomly generate decision variables treated as the random solution. Next, the fitness of the solution can be obtained by a FLAC^{3D} evaluation. The random solution and the corresponding fitness are treated as a sample. After the collection of some samples, a GP model is constructed for the given dataset. Once the trained model is obtained, we can directly use the GP model instead of FLAC^{3D} to forecast more adaptive decision variables. Finally, the current best solution is evaluated by FLAC^{3D} and added to the training dataset instead of the worst particle. If the fitness is unsuccessful, a new loop starts until the required minimal solution is found. This new back analysis optimization method is called GP-PSO-FLAC^{3D}, and its structure is given in Fig. 6. The specific implementation steps are as follows:

Step 1: Establish the numerical calculation model for a tunnel using FLAC^{3D}. A certain kind of rock mass rheological constitutive model is chosen, and the parameters of the model are regarded as the decision variables. Select the monitoring points and monitoring time. Establish the fitness function based on Eq. (1).
Step 2: Determine the dimension of PSO according to the number of decision variables. The first and the $(2 + p)th$ generation particles of the outer cycle are randomly initialized based on the particle swarm rules. Next, the random solutions are imported into FLAC^{3D} as constitutive model parameters for fitness evaluation. If the minimum fitness meets the required accuracy, the algorithm is stopped. The particle of the minimum fitness is the optimal solution;

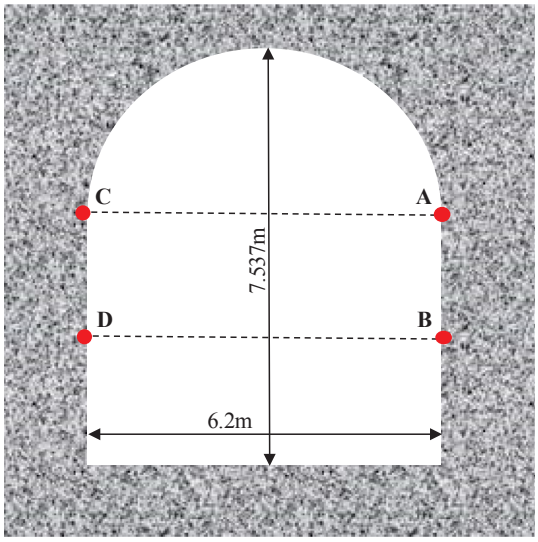

Fig. 10. Dimension and monitoring lines of section BK14 + 599.

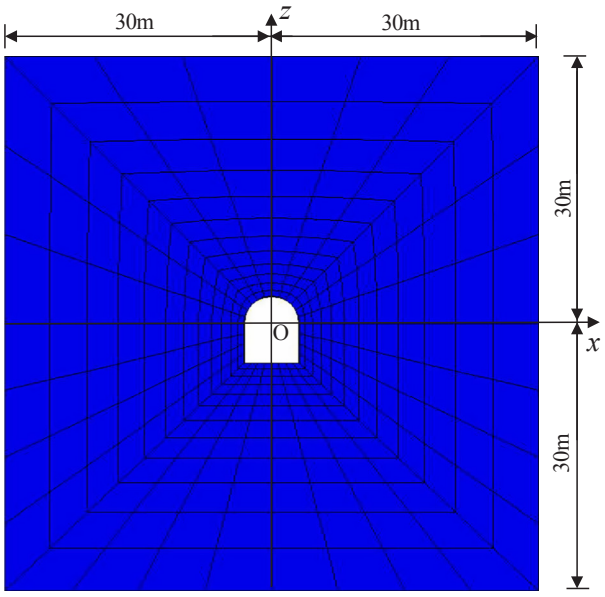

Fig. 11. Finite difference mesh of section BK14 + 599.

otherwise, the program goes to the next step.

Step 3: When the parameter $p = 0$, the original training datasets are built based on the information of the first- and second-generation particles. If the parameter $p \neq 0$, the training datasets are dynamically updated. Subsequently, the particle with the minimum fitness in the training datasets is regarded as the historical optimal solution.

Step 4: The method goes into the inner cycle. According to the PSO rules, k generation particles of the inner cycle can be produced. The nonlinear mapping relationship between the decision variables and fitness is established by using the GP machine learning method by studying the training datasets. The learned GP model is then used to replace FLAC^{3D} to evaluate the *kth* generation fitness. The particle of

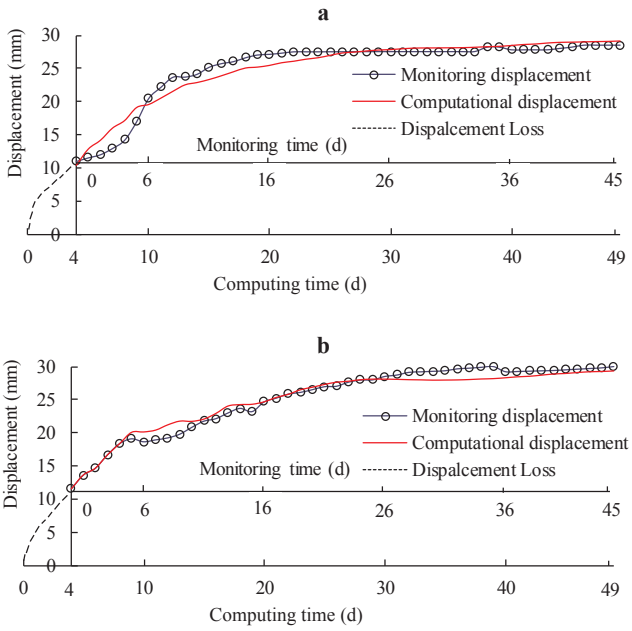

Fig. 12. Comparison between the computational displacement and monitoring displacement of monitoring lines of section BK14 + 599 (**a:** line AC; **b:** line BD).

the minimum fitness for k times is found through circulation, and this value is chosen as the optimal solution based on the GP predictive value.

Step 5: It is considered that there must be a certain error between the predictive value of the optimal solution and the real solution. Thus, the particle corresponding to the optimal solution is imported into FLAC^{3D} to obtain the real fitness. The real fitness obtained with the historical optimal solution *gbest* is compared, and the smaller value is the optimal solution of the current iteration step. This particle replaces the worst particle in the training datasets to dynamically update the training datasets.

Step 6: Judge the precision of the current optimal solution. If the precision satisfies the required accuracy, the method is stopped; otherwise, the $(2 + p)th$ generation particles of the outer cycle are produced and evaluated by FLAC^{3D}. Next, all the samples between the particles of this generation and the original training datasets are ranked from small to large based on their fitness. The same numbers of samples as in the original training datasets, which have a smaller fitness, are chosen to build new training datasets. The program goes to **Step 3.**

Based on the implementation steps described above, a MATLAB program, which can call FLAC^{3D} by an interface routine, is developed for the GP-PSO-FLAC^{3D} method.

4. Case study

To certify the performance of GP-PSO-FLAC^{3D}, simulations are performed for a tunnel. The proposed method is compared to the standard PSO method by evaluating the precision and efficiency. The mesh of one-fourth of the tunnel is shown in Fig. 7. The diameter of the tunnel is 10 m. The surrounding rock mass along the x and z directions

Table 9
Comparison of the results obtained with PSO-FLAC^{3D} and GP-PSO-FLAC^{3D} for section BK14 + 599.

Method	μ	E (GPa)	η (10^4GPa·d)	The times of fitness evaluation	Computing time (s)
PSO-FLAC^{3D}	0.201	10.125	5.955	5597	18,243
GP-PSO-LAC^{3D}	0.263	10.295	7.958	1438	4602

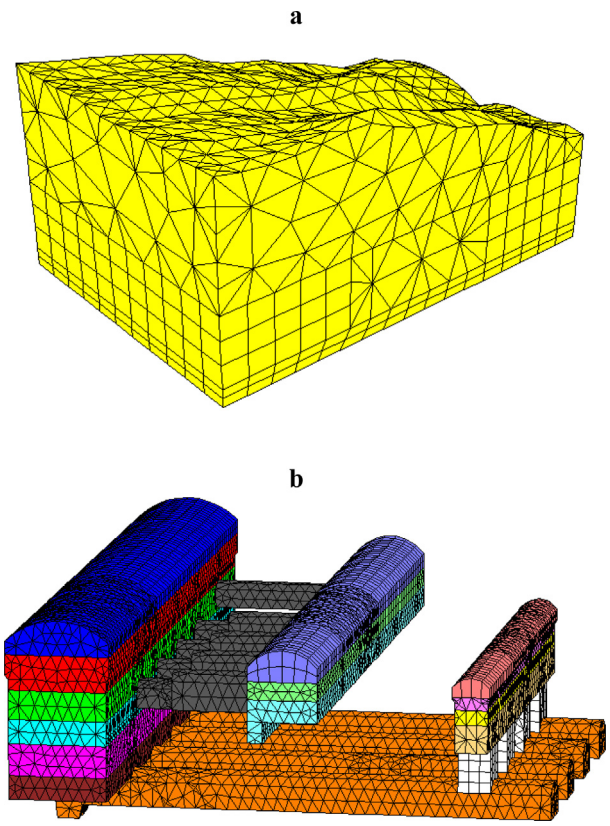

Fig. 13. Designed computational region and large group of underground caverns for the Taian pumped storage power station (**a:** 3D finite difference element model of the computational region; **b:** 3D finite difference element model of the caverns).

are 45 m. The thickness of the surrounding rock mass along the y direction is 5 m. The lithological character is homogeneous, and the initial stress of the surrounding rock mass is as follows: $\sigma_x = 30$ MPa, $\sigma_y = 10$ MPa, and $\sigma_z = 20$ MPa. The constitutive model is the classic viscoelastic model. The model has three parameters, namely, Poisson's ratio μ, elasticity modulus E and viscosity coefficient η. Thus, the dimension of PSO is three. As an example, 5 monitoring points—a, b, c, d and e—are selected to establish the optimization objective function (Fig. 7), and their detailed locations are listed in Table 4. The real parameters of the constitutive model are assumed to be $\mu = 0.25$, $E = 5.0$ GPa, and $\eta = 10$ GPa·d. The computing time is 10 days, and the monitoring time is 6 days, which means that the displacement loss is generated in 4 days. The objective function, also called the fitness function, can be determined from Eq. (1). Here, $m = 6$ d, $n = 5$, and the search intervals for the decision variables are $0.1 \le \mu \le 0.4$, 3.0

Table 10
Corresponding excavation stages and steps for the Taian pumped storage power station.

Number of stage	Main powerhouse	Main transformer cavern	Surge chambers
1	1	1	1
2	2, 3, 4	2, 3	2, 3, 4
3	5, 6, 7	—	5

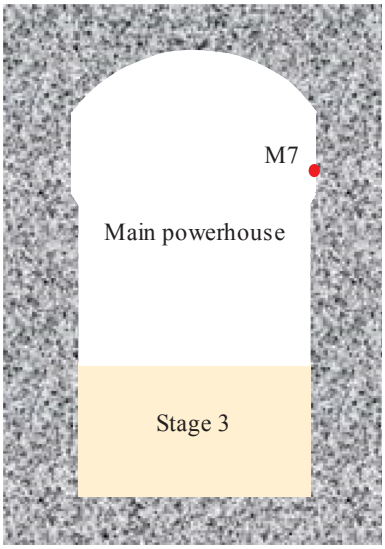

Fig. 15. Location of monitoring point M7 in section ML0+15 for the main powerhouse of the Taian pumped storage power station.

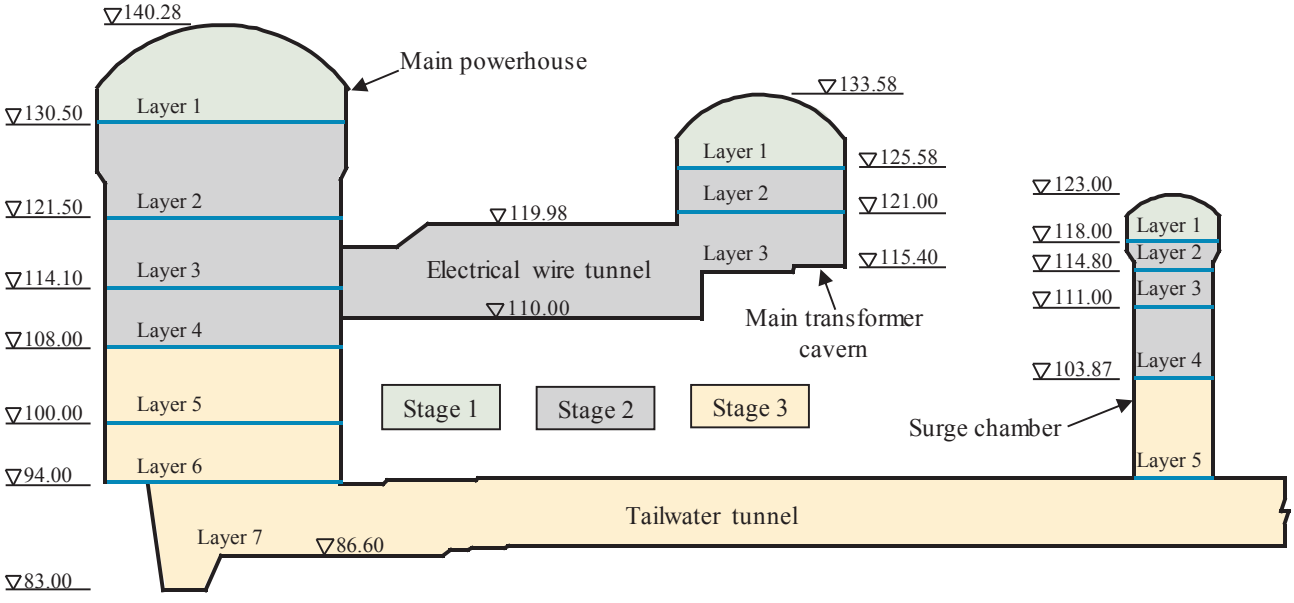

Fig. 14. Sketch map of layering excavation for the Taian pumped storage power station.

Table 11
Comparison of the results obtained with PSO-FLAC^{3D} and GP-PSO-FLAC^{3D} for section ML0 + 15.

Method	μ	E (GPa)	η (10^4GPa·d)	The times of fitness evaluation	Computing time (s)
PSO-FLAC^{3D}	0.182	3.467	6.514	360	252,360
GP-PSO-FLAC^{3D}	0.221	3.960	5.749	44	30,932

GPa $\leq E \leq$ 7.0 GPa, and 8.0 GPa·d $\leq \eta \leq$ 12.0 GPa·d.

The required accuracy is $f < 1 \times 10^{-5}$. The configuration settings of the PSO used for performing the experiments are described as follows: $D = 3$, $N = 30$, $lb = [0.1,3.0,8.0]$, $ub = [0.4,7.0,12.0]$, $\boldsymbol{v}_{\max} = [0.01,0.01,0.01]$, $c_1 = c_2 = 2$, and $t_{max} = 500$. The parameters of the PSO for GP-PSO algorithm are the same as those for the standard PSO method. The other parameter for GP-PSO is $k = 10$. The initial hyperparameters of the GP are $\ln\boldsymbol{l} = [-1,-1,-1]$, $\ln\sigma_f = -1$, and $\sigma_n = 1 \times 10^{-6}$.

For the comparisons to be fair, the two methods are independently run 5 times. The final times of the fitness evaluation are the average times. The computer on which the program is run has the following configuration: Intel(R) Core(TM) i7-4790 K CPU @ 4.00 GHz processor and 8.00 GB memory. Table 5 presents the reasonable results considering the displacement loss. The relative errors for all the mechanical parameters obtained by the two methods are acceptable, of which the maximum relative errors are both below 5%. It can also be seen that the total numbers of real fitness evaluations using GP-PSO-FLAC^{3D} and PSO-FLAC^{3D} are 185 and 600, respectively. The proposed method has a significant advantage in terms of the cost compared with the original method; the cost for the proposed method is nearly 3.3 times lower than that of PSO. To provide a visual and detailed comparison of the precision of GP-PSO-FLAC^{3D}, a graph comparing the computed displacement and monitored displacement for the 5 monitoring points is shown in Fig. 8, from which we can see that the computational displacement curve agrees well with the monitoring displacement curve. Table 6 presents a comparison between the computational displacement loss and assumed displacement loss. The maximum relative error among the 5 monitoring points is 0.609% for point a, and the minimum relative error is 0.059% for point b. The average relative error is only 0.363%, indicating that the proposed method is feasible, and it can obtain the reasonable displacement loss by fitting the monitoring displacement curve.

To study the influence of the monitoring time on the accuracy of predicting the displacement loss, the monitored displacements for 4 and 2 days, which correspond to 6 and 8 days after excavation, are also used to predict the displacement loss for 5 monitoring points. Because the program has a smaller monitored displacement to establish the fitness function, it cannot attain a higher accuracy. Therefore, the required accuracy is changed to $f < 1 \times 10^{-4}$, and the other parameters are the same as those mentioned above. The prediction results are presented in Table 7, from which we can see that the accuracy of predicting the displacement loss decreases with the monitoring time. For the displacement monitored during the last two days, the relative errors for monitoring points a and b are more than 2%; therefore, the reliability of the computational results is relatively low. Moreover, to study the influence of the number of monitoring points on the accuracy of predicting the displacement loss, 1, 3 and 5 monitoring points for a monitoring time of 6 days are selected for comparison, and the comparison results are presented in Table 8. The maximal relative error for 1 monitoring point is 2.436%, that for 5 points is only 0.878% and that for 3 points is 2.071% which is an approximately median value of the relative error. In addition, the average relative errors for these numbers of points are 1.687%, 0.598% and 1.099%. This indicates that a larger number of monitoring points used for prediction leads to better results being obtained for the displacement loss.

5. Engineering application

5.1. The auxiliary tunnel for the Jinping II power station

The Jinping II hydropower station, located in Southwest China's Sichuan Province, stands in the main stream of the Yalong River to make the most of the natural water head difference for generating electrical energy. It has four conveying tunnels with a maximum depth of 2550 m, and it is regarded as a large underground water power project with superdeep and long tunnels. To ensure the safety of the tunnel construction, two auxiliary tunnels A and B are excavated to explore the geological conditions in advance (Fig. 9a) (Zhang et al., 2012). Most parts of the auxiliary tunnels are located in a region with a high geostress, and thus, the stress of the surrounding rock is acutely released after excavation. Taking section BK14 + 599 of auxiliary tunnel B as an example, the PSO-FLAC^{3D} and GP-PSO-FLAC^{3D} methods are used to perform the back analysis of the displacement loss of the surrounding rock based on the monitored displacement data.

The basic characteristics of section BK14 + 599 include T^5_{2y}, a gray-white-colored, striped, coarse lamellar and fine-grained marble, and a black-colored, laminar and fine-grained marble. The initial geostress conditions were $\sigma_x = 35.622$ MPa, $\sigma_y = 27.772$ MPa, and $\sigma_z = 41.252$ MPa (Chen et al., 2007). The dimensions of the tunnel and the layout of the monitoring points are shown in Fig. 10. This section was excavated on 10th September, and the monitoring points were assembled on 14th September 2005. The total monitoring time was 45 days. Thus, the displacement loss was generated from 10th to 14th September.

The numerical meshing is shown in Fig. 11. The horizontal x-direction and vertical z-direction of the model are 60 m each, and the unit thickness is taken along the y-direction of the tunnel axis. The measured convergent displacement of measurement lines AC and BD are used to establish the fitness function according to Eq. (1). Here, $m = 45$ d, $n = 4$, and the search intervals for the decision variables are $0.1 \leq \mu \leq 0.3$, 1.0 GPa $\leq E \leq$ 12.0 GPa, and 1.0×10^4 GPa·d $\leq \eta \leq 12.0 \times 10^4$ GPa·d. The termination criterion is accuracy $f < 1 \times 10^{-1}$ and the other relevant parameter settings of the two methods are the same as in the above case.

The optimal solutions and the computing time obtained from the above two methods are summarized in Table 9. With the same stopping accuracy, it is observed that GP-PSO-FLAC^{3D} consumed 4602 s and achieved a much shorter prediction than PSO-FLAC^{3D}, which consumed 18,243 s. This result indicates that if we choose different methods to back analyze this problem, the proposed method requires only approximately 1.5 h, while the traditional method may cost more than 5 h. The proposed method thus has the typical advantages of a low computational cost and a high computational efficiency. A plot of the computed displacement and actual measured displacement for GP-PSO-FLAC^{3D} is presented in Fig. 12. The displacement loss of line AC is 10.45 mm, which accounts for 36% of the total displacement. Meanwhile, the displacement loss of line BD is 11.46 mm, which occupies 38% of the total displacement. If only the monitored displacement, which is far less than the actual total displacement, is used to guide the tunnel excavation or evaluate the stability of the surrounding rock, a potential risk may be posed to the construction and operation safety of the tunnel.

Therefore, due to the large buried depth and large elastic deformation after excavation, the displacement loss of the surrounding

rock for the conveying and the auxiliary tunnels cannot be ignored, more attention should be paid to evaluating the stability of the surrounding rock.

5.2. Main powerhouse of the Taian pumped storage power station

The Taian pumped storage power station, which is located in Shandong Province of North China approximately 70 km south of Ji'nan (the capital of Shandong Province), is a daily regulating power station that regulates the peak for the power grid (Fig. 9b). There are four electricity generators with a total installed capacity of 1000 MW. A large group of underground caverns that include the main powerhouse, main transformer cavern, surge chambers, four electrical wire tunnels and four tailwater tunnels is located in the right bank of the mountain, the computational region of which is shown in Fig. 13a. The corresponding 3D finite difference model contains the main powerhouse, main transformer, main transformer cavern and other main structures, and it includes 687,133 elements and 191,323 nodes (Fig. 13b).

The main powerhouse is 180 m long, 25.9 m wide, and 53.675 m high with an axis azimuth of N40°W; it was excavated in fresh mixed granite at a depth approximately ranging from 210 m to 240 m. It was been excavated in three stages containing seven steps (Fig. 14). The correspondence between the stage and step is presented in Table 10. We select the second stage as an engineering application. The initial geostress is determined by comparing three common field measurements, including the Kaiser effect of the acoustic emission method (Holcomb, 1993), the overcoring method (Sjoberg et al., 2003) and the hydraulic fracturing method (Haimson and Cornet, 2003). The maximum horizontal principal stress is 12 MPa at a direction of N70°E, and the minimum horizontal principal stress is 7 MPa. Monitoring point M7 located on section ML0 + 15 is selected to establish the fitness function according to Eq. (1) (as shown in Fig. 15). The monitored displacement after 79 days and the displacement loss after 5 days lead to $m = 79$ d and $n = 1$ for the fitness function. In addition, $N = 10$ for the PSO-FLAC^{3D} and GP-PSO-FLAC^{3D} methods, while the other parameters for the two methods are the same as those in Section 5.1.

The performances of both methods are compared in terms of the computational efficiency in Table 11. It can be seen from Table 11 that the total number of FLAC^{3D} evaluations for PSO-FLAC^{3D} is much more than that for GP-PSO-FLAC^{3D} by approximately 8 times. In addition, more attention must be focused on the computational time. Currently, one numerical evaluation for this complex large group of underground caverns costs more than 10 min. Thus, the total time for PSO-FLAC^{3D} is more than 70 h, which may be difficult to accept; however, the time for GP-PSO-FLAC^{3D} is nearly 8.5 h, which means that the proposed method can reduce the computational time considerably, especially for complex engineering problems. Meanwhile, the displacement loss obtained for M7 is 0.76 mm, which constitutes more than 14% of the total displacement. From this example, we can see that the displacement loss is less than that in the example shown in Section 5.1 because of the smaller geostress. However, this also indicates that the proposed method is suitable for engineering under not only high geostress conditions but also ordinary geostress conditions.

However, there are some attentions should be paid to the proposed method in practical engineering applications. First, the reliability of the actual monitored displacement has important influence on the accuracy of the back analysis results. Therefore, it would be necessary to identify the actual monitored displacement and to choose the credible data to use; this is somewhat dependent on the experience of engineers. In addition, the determination of the range for the back analysis parameters will also depend on experience to some extent. If over-range parameter values are used, the computational cost will increase, while for setting appropriate ranges for the parameters, the efficiency of the method can be improved.

Finally, as mentioned in Section 4, it is worth noting that the proposed method is more applicable to the underground rock mass engineering whose actual monitored displacement is obtained in time after excavation. If the displacement monitoring equipments are assembled too late, the applicability of the proposed method will be reduced and the accuracy of the prediction will decline.

6. Conclusions

The consideration of the displacement loss is critical to realize a reasonable evaluation of the stability of the surrounding rock mass for underground engineering. This paper proposes a new method that considers the displacement loss. Based on the monitored displacement, the displacement loss can be predicted by the optimization back analysis method, and the reasonable mechanical parameters of the surrounding rock mass can also be obtained simultaneously. The main conclusions can be summarized as follows:

(1) A novel displacement back analysis method considering the displacement loss is developed. Compared with traditional methods that do not consider the displacement loss, the proposed method can obtain more reasonable mechanical parameters of rock masses.
(2) It is important to reduce the number of real numerical evaluations when performing optimization back analysis for the displacement loss, as it is a time-consuming process. A new hybrid optimization algorithm for solving computationally expensive back analysis problems is proposed based on the GP and PSO. The results show that the proposed method is feasible. Compared with former optimization back analysis methods, this method can dynamically update the training datasets for the GP, thereby overcoming the disadvantage of overly relying on the initial learning samples. In addition, it has the merits of a high precision and high computational efficiency.
(3) The case study shows that the back analysis accuracy for the displacement loss is reduced with a decrease in the monitoring duration and number of monitoring points. Thus, in reality, monitoring instruments should be established as early as possible, and as many monitoring points as possible should be selected to further improve the reliability of the obtained displacement loss.
(4) The displacement loss back analysis results for section BK14 + 599 of auxiliary tunnel B in the Jinping II hydropower station show that the displacement loss occupied more than one-third of the total displacement. Due to the high geostress, the surrounding rock of deep underground engineering generates a large elastic deformation in a short time after excavation. Therefore, to accurately evaluate the stability or back analyze the parameters of the surrounding rock, the displacement loss should be considered. An engineering application of the main powerhouse of the Taian pumped storage power station indicates that the proposed method can also obtain the displacement loss in engineering processes under ordinary geostress conditions.

For the convenience of engineering applications, only the displacement loss for the classic viscoelastic constitutive model was investigated in this paper. To apply this method to different projects, considering the characteristics of the surrounding rock, a suitable constitutive model of the rock should be selected. In addition, the deformation of the surrounding rock is affected by many factors, such as the excavation method, excavation footage and support. Accordingly, the influences of various factors on the displacement loss should be discussed in further research.

Acknowledgements

The authors would like to acknowledge the financial support from the National Natural Science Foundation of China under Grant No. 51869003, 51409051 and 51568014. The work in this paper was also supported by the Open Fund of State Key Laboratory of Geohazard

Prevention and Geoenvironment Protection (Chengdu University of Technology) under Grant No. SKLGP2017K022, the Systematic Project of Guangxi Key Laboratory of Disaster Prevention and Structural Safety under Grant No. 2019ZDK023 and the Guangxi Natural Science Foundation under Grant No. 2016GXNSFGA380008.

References

Barton, N., Lien, R., Lunde, J., 1974. Engineering classification of rock masses for the design of tunnel support. Rock Mech. 6, 189–236.

Beiki, M., Majdi, A., Givshad, A.D., 2013. Application of genetic programming to predict the uniaxial compressive strength and elastic modulus of carbonate rocks. Int. J. Rock Mech. Min. Sci. 63, 159–169.

Berti, M., Bertello, L., Bernardi, A.R., Caputo, G., 2017. Back analysis of a large landslide in a flysch rock mass. Landslides 14, 2041–2058.

Bieniawski, Z.T., 1984. Rock Mechanics Design in Mining and Tunnelling. AA Balkema, Rotterdam.

Brigham, J.C., Aquino, W., 2007. Surrogate-model accelerated random search algorithm for global optimization with applications to inverse material identification. Comput. Methods Appl. Mech. Eng. 196, 4561–4576.

Cai, M., 2011. Rock mass characterization and rock property variability considerations for tunnel and cavern design. Rock Mech. Rock Eng. 44, 379–399.

Cai, M., Morioka, H., Kaiser, P.K., Tasaka, Y., Kurose, H., Minami, M., Maejima, T., 2007. Back-analysis of rock mass strength parameters using AE monitoring data. Int. J. Rock Mech. Min. Sci. 44, 538–549.

Cai, M.F., He, M.C., Liu, D.Y., 2002. Rock Mechanics and Engineering. Science Press, Beijing.

Chen, B.R., Feng, X.T., Huang, S.L., Yang, C.X., Zhang, C.Q., 2007. Inversion of viscoelasto-plastic parameters based on fast Lagrangian analysis of continuum-parallel particle swarm algorithm and its application. Chin. J. Rock Mech. Eng. 26, 2517–2525.

Digalakis, J., Margaritis, K., 2004. Performance comparison of memetic algorithms. Appl. Math. Comput. 158, 237–252.

Eberhart, R.C., Kennedy, J., 1995. A new optimizer using particle swarm theory. In: Proceedings of the Sixth International Symposium on Micro Machine and Human Science. Nagoya, Japan, pp. 39–43.

Evers, G.I., Ghalia, M.B., 2009. Regrouping particle swarm optimization: A new global optimization algorithm with improved performance consistency across benchmarks. In: IEEE International Conference on Systems, Man and Cybernetics. San Antonio, USA, pp. 3901–3908.

Farias, M.M.D., Junior, A.H.M., Assis, A.P.D., 2004. Displacement control in tunnels excavated by the NATM: 3-D numerical simulations. Tunn. Undergr. Space Technol. 19, 283–293.

Feng, X.T., Zhang, Z.Q., Sheng, Q., 2000. Estimating mechanical rock mass parameters relating to the three gorges project permanent shiplock using an intelligent displacement back analysis method. Int. J. Rock Mech. Min. Sci. 37, 1039–1054.

Feng, X.T., Zhang, Z.Q., Yang, C.X., Lin, Y.M., 1999. Study on genetic-neural network method of displacement back analysis. Chin. J. Rock Mech. Eng. 18, 497–502.

Feng, X.T., Chen, B.R., Yang, C.X., Zhou, H., Ding, X.L., 2006. Identification of viscoelastic models for rocks using genetic programming coupled with the modified particle swarm optimization algorithm. Int. J. Rock Mech. Min. Sci. 43, 789–801.

Gao, W., 2006. Back analysis algorithm in geotechnical engineering based on particle swarm optimization. Rock Soil Mech. 5, 795–798.

Gao, W., Feng, X.T., 2005. Study on a new back analysis algorithm in geotechnical engineering based on immunized continuous and ant colony algorithm. Chin. J. Rock Mech. Eng. 24, 4266–4271.

Gioda, G., Sakurai, S., 1987. Back analysis procedures for the interpretation of field measurements in geomechanics. Int. J. Numer. Anal. Methods Geomech. 11, 555–583.

Haimson, B.C., Cornet, F.H., 2003. ISRM Suggested Methods for rock stress estimation—Part 3: hydraulic fracturing (HF) and/or hydraulic testing of pre-existing fractures (HTPF). Int. J. Rock Mech. Min. Sci. 40, 1011–1020.

Hajihassani, M., Armaghani, D.J., Kalatehjari, R., 2018. Applications of particle swarm optimization in geotechnical engineering: a comprehensive review. Geotech. Geol. Eng. 36, 705–722.

Hashash, Y., Levasseur, S., Osouli, A., Finno, R., Malecot, Y., 2010. Comparison of two inverse analysis techniques for learning deep excavation response. Comput. Geotech. 37, 323–333.

Hoek, E., Diederichs, M.S., 2006. Empirical estimation of rock mass modulus. Int. J. Rock Mech. Min. Sci. 43, 203–215.

Hao, X.J., Feng, X.T., Yang, C.X., Jiang, Q., Li, S.J., 2016. Analysis of EDZ development of columnar jointed rock mass in the Baihetan diversion tunnel. Rock Mech. Rock Eng. 49, 1289–1312.

Hensman, J., Mills, R., Pierce, S.G., Worden, K., Eaton, M., 2010. Locating acoustic emission sources in complex structures using Gaussian processes. Mech. Syst. Signal Pr. 24, 211–223.

Holcomb, D.J., 1993. General theory of the Kaiser effect. Int. J. Rock Mech. Min. Sci. & Geomech. Abstr. 30, 929–935.

Itasca, 2005. FLAC3D Version 3.0, User manual. Itasca Consulting Group Inc., Minneapolis.

Jadaliha, M., Xu, Y., Choi, J., Johnson, N.S., Li, W., 2013. Gaussian process regression for sensor networks under localization uncertainty. Signal Process IEEE Trans. 61, 223–237.

Kaiser, P.K., Zou, D., Lang, P.A., 1990. Stress determination by back-analysis of excavation-induced stress changes – A case study. Rock Mech. Rock Eng. 23, 185–200.

Karaboga, D., Basturk, B., 2008. On the performance of artificial bee colony (ABC) algorithm. Appl. Soft Comput. 8, 687–697.

Khamesi, H., Torabi, S.R., Mirzaei-Nasirabad, H., Ghadiri, Z., 2015. Improving the performance of intelligent back analysis for tunneling using optimized fuzzy systems: case study of the Karaj subway line 2 in Iran. J. Comput. Civ. Eng. https://doi.org/10.1061/(ASCE)CP.1943-5487.0000421.

Knabe, T., Schweiger, H.F., Schanz, T., 2012. Calibration of constitutive parameters by inverse analysis for a geotechnical boundary problem. Can. Geotech. J. 49, 170–183.

Levasseur, S., Malécot, Y., Boulon, M., Flavigny, E., 2010. Statistical inverse analysis based on genetic algorithm and principal component analysis: applications to excavation problems and pressuremeter tests. Int. J. Numer. Anal. Methods Geomech. 34, 471–491.

Li, F., Wang, J., Brigham, J.C., 2014a. Inverse calculation of insitu stress in rock mass using the surrogate-model accelerated random search algorithm. Comput. Geotech. 61, 24–32.

Lin, P., Liu, X.L., Chen, H.X., Kim, J.X., 2014. Ant colony optimization analysis on overall stability of high arch dam basis of field monitoring. Sci. World J. https://doi.org/10.1155/2014/483243.

Li, Y.Y., Wang, Q., Chen, J.P., Xu, L.M., Song, S.Y., 2014b. *K*-means algorithm based on particle swarm optimization for the identification of rock discontinuity sets. Rock Mech. Rock Eng. 48, 375–385.

Lu, A.Z., Zhang, N., Kuang, L., 2014. Analytic solutions of stress and displacement for a non-circular tunnel at great depth including support delay. Int. J. Rock Mech. Min. Sci. 70, 69–81.

Miro, S., König, M., Hartmann, D., Schanz, T., 2015. A probabilistic analysis of subsoil parameters uncertainty impacts on tunnel-induced ground movements with a back-analysis study. Comput. Geotech. 68, 38–53.

Mohammadi, S.D., Naseri, F., Alipoor, S., 2014. Development of artificial neural networks and multiple regression models for the NATM tunnelling-induced settlement in Niayesh subway tunnel. Tehran. Bull. Eng. Geol. Environ. 74, 827–843.

Moreira, N., Miranda, T., Pinheiro, M., Fernandes, P., Dias, D., Costa, L., Sena-Cruz, J., 2013. Back analysis of geomechanical parameters in underground works using an evolution strategy algorithm. Tunn. Undergr. Space Technol. 33, 143–158.

Ninić, J., Freitag, S., Meschke, G., 2017. A hybrid finite element and surrogate modelling approach for simulation and monitoring supported TBM steering. Tunn. Undergr. Space Technol. 63, 12–28.

Ninić, J., Meschke, G., 2015. Model update and real-time steering of tunnel boring machines using simulation-based meta models. Tunn. Undergr. Space Technol. 45, 138–152.

Ojha, R., Das, M., 2012. An adaptive approach for modifying inertia weight using particle swarm optimisation. Int. J. Comput. Sci. 9, 105–111.

Pal, M., Deswal, S., 2010. Modelling pile capacity using Gaussian process regression. Comput. Geotech. 37, 942–947.

Pirulli, M., Mangeney, A., 2008. Results of back-analysis of the propagation of rock avalanches as a function of the assumed rheology. Rock Mech. Rock Eng. 41, 59–84.

Rasmussen, C.E., 2006. Gaussian Processes for Machine Learning. MIT Press, Massachusetts.

Rechea, C., Levasseur, S., Finno, R., 2008. Inverse analysis techniques for parameter identification in simulation of excavation support systems. Comput. Geotech. 35, 331–345.

Sakurai, S., Takeuchi, K., 1983. Back analysis of measured displacements of tunnels. Rock Mech. Rock Eng. 16, 173–180.

Seeger, M., 2004. Gaussian processes for machine learning. Int. J. Neural Syst. 14, 69–106.

Sjoberg, J., Christiansson, R., Hudson, J.A., 2003. ISRM suggested methods for rock stress estimation—Part 2: overcoring methods. Int. J. Rock Mech. Min. Sci. 40, 999–1010.

Su, G.S., Yan, L.B., Song, Y.C., 2007. Gaussian process for non-linear displacement time series prediction of landslide. J. China Univ. Geosci. 18, 219–221.

Tang, Y.G., Kung, G.T.C., 2009. Application of nonlinear optimization technique to back analyses of deep excavation. Comput. Geotech. 36, 276–290.

Wang, G., Ma, Z., 2017. Hybrid particle swarm optimization for first-order reliability method. Comput. Geotech. 81, 49–58.

Wang, R.J., Li, C., Xu, J.H., Pan, L.J., 2018. Development and verification of large deformation model considering stiffness deterioration and shear dilation effect in FLAC^{3D}. Int. J. Rock Mech. Min. Sci. 28, 959–967.

Yang, C.X., Wu, Y.H., Hon, T., 2010. A no-tension elastic–plastic model and optimized back-analysis technique for modeling nonlinear mechanical behavior of rock mass in tunneling. Tunn. Undergr. Space Technol. 25, 279–289.

Yu, J.D., Hong, Y.H., Byun, Y.H., Lee, J.S., 2016. Non-destructive evaluation of the grouted ratio of a pipe roof support system in tunneling. Tunn. Undergr. Space Technol. 56, 1–11.

Zhang, C.Q., Feng, X.T., Zhou, H., Hou, J., Su, G.S., 2009. Method of obtaining loss convergence displacement and its application to tunnel engineering. Rock Soil Mech. 30, 997–1003.

Zhang, C.Q., Zhou, H., Feng, X.T., 2008. Numerical format of elastoplastic constitutive model based on the unified strength theory in FLAC^{3D}. Rock Soil Mech. 29, 596–602.

Zhang, C.Q., Feng, X.T., Zhou, H., Qiu, S.L., Wu, W.P., 2012. A top pilot tunnel preconditioning method for the prevention of extremely intense rockbursts in deep tunnels excavated by TBMs. Rock Mech. Rock Eng. 45, 289–309.

Zhao, H.B., Yin, S.D., 2009. Geomechanical parameters identification by particle swarm optimization and support vector machine. Appl. Math. Model 33, 3997–4012.